

Article

Fast and Slow Laser-Stimulated Degradation of Mn-Doped $\text{Li}_4\text{Ti}_5\text{O}_{12}$

Aleksey A. Nikiforov ¹, Dmitrii K. Kuznetsov ¹, Ralph N. Nasara ², Kaviarasan Govindarajan ³, Shih-kang Lin ^{3,4,5,6} and Dmitry V. Pelegov ^{1,*}¹ Institute of Natural Sciences and Mathematics, Ural Federal University, Ekaterinburg 620002, Russia² Graduate School of Engineering, Kyoto University, Kyoto 615-8510, Japan³ Department of Materials Science and Engineering, National Cheng Kung University, Tainan 70101, Taiwan⁴ Program on Smart and Sustainable Manufacturing, Academy of Innovative Semiconductor and Sustainable Manufacturing, National Cheng Kung University, Tainan 70101, Taiwan⁵ Hierarchical Green-Energy Materials (Hi-GEM) Research Center, National Cheng Kung University, Tainan 70101, Taiwan⁶ Core Facility Center, National Cheng Kung University, Tainan 70101, Taiwan

* Correspondence: dmitry.pelegov@urfu.ru

Abstract: Lithium titanate ($\text{Li}_4\text{Ti}_5\text{O}_{12}$) is a commercial anode material used for high-power and long-lifespan lithium batteries. The key drawback of this material is its low electronic conductivity. Although doping is commonly used to solve this problem, the introduction of dopants also diminished lattice stability. In this work, we studied fast and slow laser-induced degradation processes of single Mn-doped lithium titanate particles and proposed a physicochemical model of their degradation mechanism. We suppose that the preferable route of LTO alteration is the formation of amorphous phases rather than crystalline decomposition products. Our results may be useful for not only developing a nondestructive characterization tool utilizing Raman spectroscopy but also for understanding other degradation processes, including thermal alteration and structural changes caused by the intercalation/deintercalation cycles of lithium ions.

Keywords: lithium titanate; Raman spectroscopy; laser-matter interaction; laser ablation; amorphization

**Citation:** Nikiforov, A.A.; K.

Kuznetsov, D.; Nasara, R.N.;

Govindarajan, K.; Lin, S.-k.; Pelegov,

D.V. Fast and Slow Laser-Stimulated

Degradation of Mn-Doped $\text{Li}_4\text{Ti}_5\text{O}_{12}$.*Batteries* **2022**, *8*, 251. [https://](https://doi.org/10.3390/batteries8120251)doi.org/10.3390/batteries8120251

Academic Editor: Sylvain Franger

Received: 27 October 2022

Accepted: 16 November 2022

Published: 22 November 2022

Publisher's Note: MDPI stays neutral with regard to jurisdictional claims in published maps and institutional affiliations.



Copyright: © 2022 by the authors. Licensee MDPI, Basel, Switzerland. This article is an open access article distributed under the terms and conditions of the Creative Commons Attribution (CC BY) license (<https://creativecommons.org/licenses/by/4.0/>).

1. Introduction

Raman spectroscopy is a common characterization tool in both chemistry and physics, and its invention in 1928 became an important landmark for modern material science [1]. However, the peculiarities of laser–matter interactions during Raman measurements have not been extensively studied. The laser-induced degradation during Raman measurement was observed in various electrode materials. The most detailed studies were performed for LiFePO_4 with olivine structure [2–7]. Moreover, laser-induced processes have been described in LiCoO_2 [8,9], $0.6\text{Li}[\text{Li}_{0.33}\text{Mn}_{0.67}]\text{O}_2$ – $0.4\text{Li}[\text{Mn}_{0.3}\text{Ni}_{0.45}\text{Co}_{0.25}]\text{O}_2$ [10], LiMn_2O_4 [11], and manganese oxides [12], but $\text{Li}_4\text{Ti}_5\text{O}_{12}$ with defect structures was considered robust against laser irradiation during Raman measurement. In this work, we examined laser-induced processes in Mn-doped lithium titanate ($\text{Li}_{3.95}\text{Mn}_{0.05}\text{Ti}_5\text{O}_{12}$, LTO), a negative electrode material for lithium batteries. To the best of our knowledge, this is the first report on laser-induced degradation of doped LTO.

This work provides insights into fast and slow laser-induced degradation processes. We believe this may help to improve the design of in-situ Raman measurements, since laser-induced processes can continue for extended periods and interfere the studied electrochemical processes. Thus, the influence of slow laser-induced processes becomes crucial for an accurate interpretation of the results obtained during prolonged in-situ Raman measurements. In addition, this work illustrates the advantages of single particle approach to Raman spectroscopy and sheds light on a difference of laser-induced processes

in Mn-doped LTO (this work) and LFP [7]. Besides the improvement of Raman studies, the results of this work can be used for better understanding of the wide range of degradation processes, including thermal alteration and structural changes caused by the intercalation/deintercalation cycles of lithium ions.

2. Materials and Methods

2.1. Sample Synthesis

Mn-doped LTO was synthesized using the solid-state method with Li_2CO_3 , TiO_2 , and MnO_2 as precursors. An excess of 5% Li_2CO_3 was added to compensate for Li volatilization during the heating process. The precursors were mixed in a stoichiometric ratio using ball milling at 600 rpm for 30 min. Then, the precursor mixture was heated at 720 °C for 1 h and 850 °C for 8 h with a 5 °C per minute heating rate in an air atmosphere to obtain the final product, Mn-doped LTO. The target stoichiometric presentation was $\text{Li}_{3.95}\text{Mn}_{0.05}\text{Ti}_5\text{O}_{12}$, but the rigorous study of sites occupancy is outside the scope of this article and therefore not performed. The discussion of lattice parameters and properties of Mn-doped LTO can be found in papers [13–16].

2.2. Sample Preparation, Visualization, and Measurements

To obtain a set of single particles, we used a dry deposition procedure by which the powder sample was deposited and gently distributed over a copper substrate, followed by dry air blowing to remove aggregates. The dry deposition method, contrary to wet deposition, helps to avoid the formation of an organic layer after drying out the liquid phase of suspension (for example, isopropyl alcohol). A copper substrate was used to minimize the contribution of the substrate to the measured spectrum. Regular laser-made marks together with a unique pattern of deposited particles and aggregates were used to accurately locate the particles, study the same particle using different methods, and perform a series of repeated measurements. The morphology of the particles was imaged using scanning electron microscopy (SEM, Carl Zeiss Auriga) with an accelerating voltage of 5 kV and a maximum resolution of 1–2 nm.

Raman measurements were conducted using a confocal Raman microscope (WiTec Alpha 300 AR). We used the 633 nm laser excitation, 100x objective with NA = 0.75. In addition to the 633 nm laser, we also tried 488 nm laser and found that the excitation at 633 nm provides more intense Raman spectra for LTO, which is important for submicron single particle measurements. The spectral measurements were performed using 600 grids per mm grating with an average spectral resolution of 1.9 cm^{-1} . Single spectra were measured with a series of 5 accumulations (20 s each). The deconvolution of the Raman spectra was performed in Peak Fit 4.0 using the Lorentz area functions. The laser radiation power was adjusted by a precision screw blocking the optical path and with power value control by Ophir Vega.

Between measurements sample were stored in air at room temperature and the relative humidity of about 10%.

3. Results

In this work, we report the results of two series of repeated Raman spectra measurements. Both series utilized a single-particle approach with a correlative study of the characterization of the same particles by Raman spectroscopy and SEM. The first series allowed us to reveal the effects of laser-induced degradation in doped LTO and provided insights into fast and slow degradation processes. The second series was used to verify the results obtained.

3.1. First Series

The first series of experiments comprised two parts—initial and repeated measurements of Raman spectra for several single particles of submicron sizes. The initial experiment included two consecutive measurements using laser powers of 2.2 and 4.9 mW. Seven

of the measured particles had relatively intense Raman spectra with five main characteristic Raman bands typical for LTO [17–20]: two $F_{2g}(\text{TiO}_6)$ at 230 cm^{-1} and 272 cm^{-1} , $F_{2g}(\text{LiO}_6)$ at 336 cm^{-1} , $E_g(\text{LiO}_4)$ at 426 cm^{-1} and $A_{1g}(\text{TiO}_6)$ at 674 cm^{-1} (Figure 1). Additional minor bands were obtained at 382 , 520 , 588 , and 740 cm^{-1} . These bands are not attributed to a specific vibration type but are common for LTO [21]. All these seven particles did not exhibit any sign of laser-induced decomposition, even at the highest laser power.

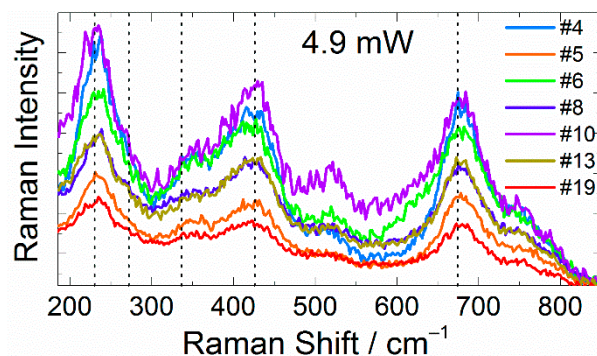


Figure 1. Raman spectra of seven individual particles. The dotted lines indicate the positions of the main characteristic LTO bands. Probing laser power: 4.9 mW.

About two months after the initial experiment, we repeated Raman spectra measurements for the same seven particles but using a wider range of probing laser power (0.09, 0.23, 0.35, 0.65, 1.2, 2.2, 3.2, 4.1, 4.6, and 4.9 mW). The analysis of the obtained results revealed three groups of particles: stable (particles #4 and #8); degraded during repeated measurement (particles #5 and #10); and degraded between measurements (particles #6, #13, and #19).

In the case of stable particles, particles #4 (Figure 2a) and #8 (Figure S1a), the repeated Raman spectra showed lower intensities but still contained all the characteristic bands of LTO. Besides lower intensity, the repeated spectra for both particles demonstrated a larger Rayleigh peak shoulder and more intense band at about 520 cm^{-1} (rescaled Raman spectra are shown in Figure S2a,b).

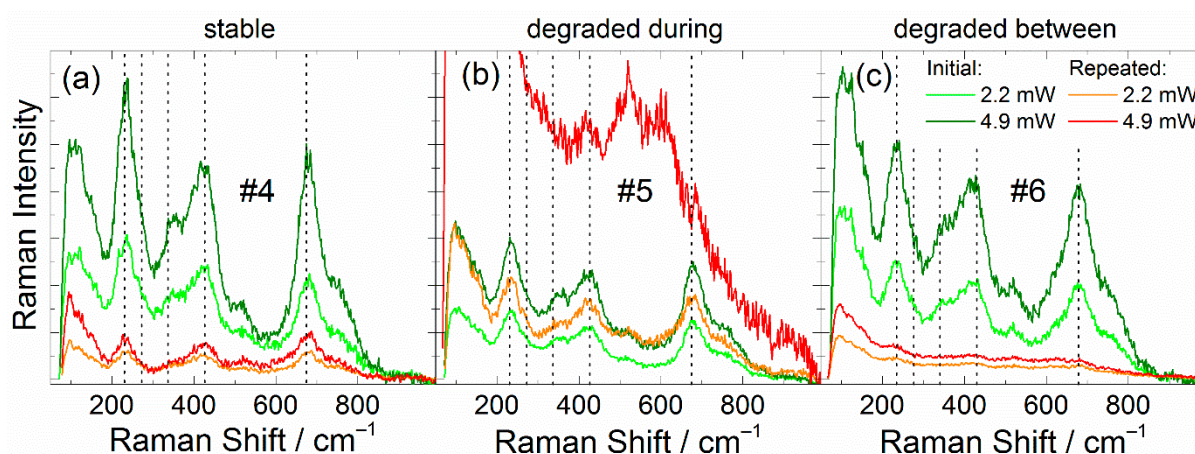


Figure 2. Raman spectra measured at two-month intervals for (a) “stable” particle #4, and (b) particle #5, degraded during repeated measurement, and (c) particle #6, degraded between initial and repeated measurements.

Particles #5 (Figure 2b) and #10 (Figure S1b) degraded during the repeated measurements as the probing laser power increased. At moderate values of the laser power, the typical Raman spectra of LTO were obtained, thus revealing no signs of degradation. The further laser power increase initiated LTO degradation. Particle #5 degraded at 4.1 mW,

and particle #10 degraded at 4.9 mW (Figure S3). During the degradation, the Raman intensity increased, and two new bands near 530 and 610 cm^{-1} became dominant, while the characteristic bands of LTO weakened (Figures 2b and S1b).

The Raman spectra of particles #6, #19, and #13, also degraded but at stages between initial and repeated measurements (Figures 2c and S1c,d). The Raman spectra of the degraded particles were similar to those degraded during measurements but with much lower intensity. The significant difference between the initial and repeated measurements allowed us to reveal the degradation process or a series of processes, which happened between these two experiments.

In addition to the alteration of Raman spectra for particles #5 and #10, the comparison of their SEM images obtained before the initial measurement and after the repeated measurement revealed numerous nanoobjects around both LTO particles, which degraded during the repeated measurement, and these nanoobjects were not observed for other particles (Figure 3). Such SEM patterns are typical for laser ablation; however, in this case, the formation of ablation products was not accompanied by visible particle damage. Both particles #5 and #10 did not lose their integrity and retained their shapes. The SEM images of particles #4 and #8 (stable particles), as well as particle #6, which degraded between the initial and repeated measurements, did not reveal nanoobjects around the particles (Figure 3). Please note that SEM images of the single LFP did not reveal such nanoobjects around the decomposed particles [7].

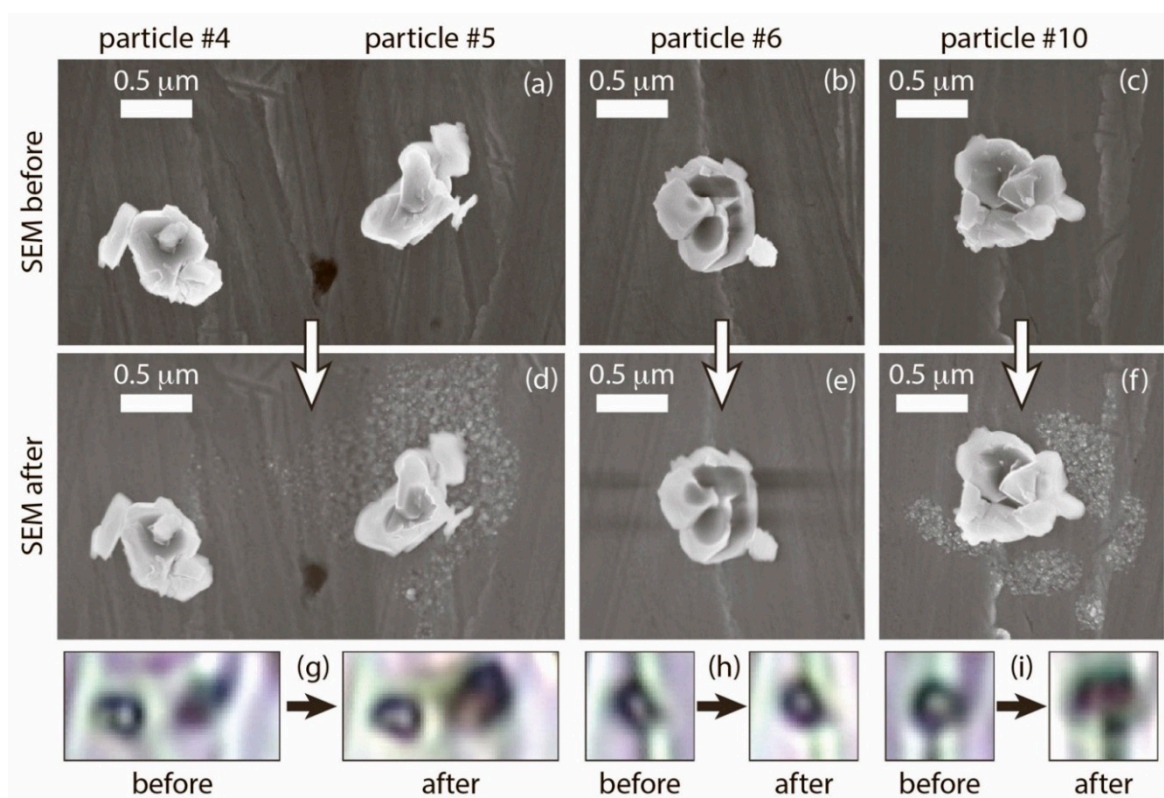


Figure 3. Particle morphology before and after the repeated action of laser irradiation, visualized by SEM (a–f) and optical microscopy (g–i). The images in the top row (a–c) were obtained before the initial Raman spectra measurements. The images in the middle row (d–f) were obtained after the repeated Raman spectra measurements. The height of the optical images in the bottom layer is 1.5 μm . The arrows are directed from image of particles before laser action to image of the same particles after it.

3.2. Second Series

To distinguish between the influences of laser irradiation and the ambient atmosphere on the degradation processes, the second series of measurements (five experiments performed at two-week intervals) were conducted.

We measured the Raman spectra of 20 LTO particles (numbered from #21 to #40) at a minimal laser power of 0.09 mW and obtained their SEM images to control possible laser ablation. The following experiments were performed for two sets of single particles: verification and control groups. The verification group of 10 particles was exposed to the full range of the probing laser power (mW): 0.09, 0.23, 0.35, 0.65, 1.2, 2.2, 3.2, 4.1, 4.6, 4.9, 4.1, 2.2, 0.65, 0.23, and 0.09. The control group of the other 10 particles was exposed only to the minimal laser power of 0.09 mW. After the fifth experiment, we performed the final SEM imaging for both groups. All 20 particles from both groups were stored under the same conditions on the same substrate near each other, so the difference in their degradation processes could reveal the role of laser irradiation. The results of such a repeated action of strong and weak laser irradiations are presented in Table 1.

Table 1. Comparison of degradation processes for control and verification groups (green: non-degraded particles, red: degraded between measurements, dark red: degraded during Raman measurement, and yellow: a particle with ambiguous Raman spectra). Second row helps to.

Exp.→	I		SEM	II		III		IV		V		SEM
Day→	01	05	15	16	18	29	32	57	60	71	74	101
Control group of particles (0.09 mW)	#22	Green		Green		Green		Green		Green		
	#23	Green		Green		Green		Green		Green		
	#26	Green		Green		Green		Green		Green		
	#28	Green		Green		Green		Green		Green		
	#29	Green		Green		Green		Green		Green		
	#31	Green	Green		Green		Green		Green		Green	
	#33	Green	Green		Green		Green		Green		Green	
	#36	Green	Green		Green		Green		Green		Green	
	#38	Green	Green		Green		Green	Yellow	Green		Green	
	#39	Green	Green		Green		Green	Yellow	Green		Green	
Verification group of particles (0.09–4.9–0.09 mW)	#21	Green		Yellow		Red		Red		Red		
	#24	Green		Green		Green		Red		Red		
	#25	Green		Green		Green		Red		Red		
	#27	Green		Green		Green		Red		Red		
	#30	Green	Green		Green		Green	Green		Green		
	#32	Green	Green		Yellow		Yellow		Red		Red	
	#34	Green	Green		Yellow		Red		Red		Red	
	#35	Green	Green		Yellow		Yellow		Yellow		Red	
	#37	Green	Green		Green		Red		Red		Red	
	#40	Green	Green		Yellow		Red		Red		Red	

In the control group, the Raman spectra of all ten particles showed the typical LTO peaks with no noticeable signs of degradation after more than seventy days and five measurements at low laser power (Figures S5–S14). To minimize the action of laser radiation, we used minimal power and moderate averaging, so the obtained Raman spectra were rather noisy but still interpretable.

In the verification group, nine out of ten particles degraded. Particle #30 demonstrated exceptional stability under the repeated actions of laser radiation and became the only nondegraded particle in this group (Figure S19). Particles #25 and #27 degraded between the third and fourth experiments. Particle #24 became the only one degraded directly during Raman spectra measurement with a drastic increase in Raman intensity, similar to particles #5 and #10 in the first series of measurements. The degradation of particles #21, #32, #34, #35, #37, and #40 can be hardly attributed to the specific moment or time interval since Raman spectra transformations lasted for several experiments.

To understand the physical phenomena behind the laser-induced degradation of LTO, we analyzed the dependence of band parameters on the probing laser power. Since LTO Raman spectra were shown to be dependent on temperature [17,22], this can help to estimate possible laser-induced heating in Mn-LTO. As shown in Figure S4, the increase in laser power from 0.09 to 4.9 mW did not result in a noticeable change in parameters for major and minor bands. Thus, we assumed that laser-induced heating was either absent or insignificant. Some perturbation at low laser power can be attributed to the low signal/noise ratio and the errors of peak deconvolution.

The analysis of SEM images (Figures S15–S24) showed that all ten particles from the verification group, including particle #10 (steady particle), demonstrated some amount of nanoscale objects around and above them. All ten particles from the control group had no such objects (Figures S5–S14).

4. Discussion

4.1. Interpretation of Raman Spectra after Degradation

The obtained results allowed us to assume that the laser-induced degradation process can be described as a phase transition “order” → “disorder” or, in other words, laser-induced amorphization. The intense Rayleigh peak shoulder (or bands below 200 cm^{-1}) and Raman bands near 530 and 610 cm^{-1} are rather typical for copper oxides [23,24], which could be formed due to the surface oxidation of the copper substrate. In most cases, this natural oxide layer is rather thin and provides a Raman response of low intensity. For a well-structured Mn-doped LTO particle, the Raman response from the substrate is partially blocked by the particle and suppressed by intensive LTO bands, thus exhibiting itself only by the intensive Rayleigh peak shoulder. When the particle became amorphous, the intensities of LTO bands decreased, and the response from the underneath copper oxide layer became notable. Further, chemical reactions taking place during Mn-doped LTO degradation and physical processes during ablation can accelerate the surface oxidation of the copper substrate, thus making its Raman response more intense. The argument against this explanation is the position of Raman bands since the characteristic band of copper oxide takes place at $620\text{--}630\text{ cm}^{-1}$ [23,24].

The laser-induced amorphization was consistent with the preceding growth of the band at about 520 cm^{-1} in the repeated spectra for particles #24, #25, and #28 (Figure S2a,b,e). In works [20,21,25–27], this band is attributed to the presence of defects, so the growth of its intensity could be attributed to particle degradation. In addition, we observed a similar trio of bands for Raman spectra for the single particles of LiFePO_4 and LiCoO_2 deposited on the oxidized copper substrate (Figure S25). In the case of single particles deposited on silicon and glass substrates, these bands were not observed.

Another possible explanation is that laser irradiation drastically increases surface conductivity, and the particle bulk becomes screened. Moreover, due to Mie scattering [28–30], such a core–shell particle may drastically change its properties, thus increasing its transparency and making the response from the copper oxide layer more pronounced.

An alternative explanation of laser-induced degradation is a phase transition “order” → “order” or, in other words, laser-induced decomposition. This type of stimulated phase transition was observed in LiFePO_4 [3–7,31–34] and LiCoO_2 [8]. Laser-induced decomposition means that the bands near 530 and 610 cm^{-1} may be attributed to some decomposition products. The most expected reaction is



Rutile TiO_2 has two dominating bands at about 609 cm^{-1} (A_{1g} mode) and 443 cm^{-1} (E_g mode) and a series of minor bands, including ones at 230 cm^{-1} and 690 cm^{-1} [35]. Li_2TiO_3 is characterized by the dominant band at 656 cm^{-1} and a dominant doublet at 401 cm^{-1} and 418 cm^{-1} [35]. There are two bands in-between and a few more below 400 cm^{-1} , but all of them are minor. With some modifications, rutile TiO_2 and Li_2TiO_3

can explain bands near 610 cm^{-1} and 420 cm^{-1} , but, at the same time, cannot explain the dominant band near 530 cm^{-1} and an intensive Rayleigh peak shoulder. The Raman spectra of rutile $\text{TiO}_2 + \text{Li}_2\text{TiO}_3$ mixture were given in [36], and all of them had a broad valley between 480 and 550 cm^{-1} .

Another possible candidate is anatase TiO_2 [37,38]. The dominating E_g band at about 144 cm^{-1} is narrow and usually well-resolved. It can broaden for nanoscale anatase TiO_2 , but this is accompanied by its shift toward higher wavenumbers [38], so this band cannot be confused with the Rayleigh peak shoulder. Other major bands of anatase TiO_2 are located at about 400 cm^{-1} (B_{1g}), 520 cm^{-1} (B_{1g} together with A_{1g}), and 640 cm^{-1} (E_g) and represent themselves as standalone bands. These bands can also broaden and form a broad triplet for nanoscale particles, but their positions are still poorly suited to the trio of bands 420 , 530 , and 610 cm^{-1} observed in this work.

Altogether, these considerations suggest laser-induced amorphization rather than laser-induced decomposition.

4.2. Physicochemical Model of Stimulated Degradation

Based on the results obtained, let us conclude about “fast” physical and “slow” chemical stimulated degradation processes. “Fast” degradation is induced directly by the action of laser irradiation during Raman measurement. “Slow” degradation takes place in-between measurements when laser irradiation is switched off. Two stages of the stimulated degradation of Mn-doped LTO can be explained by the combined action of the copper substrate with a water layer and the laser excitation of the system copper substrate–water–air–doped LTO particle.

4.2.1. Stimulated Amorphization

The pristine LTO is a highly reflective material with low light absorption. Its white color indicates a large bandgap, which has been generally reported between 1.8 and 3.8 V [39], prohibiting interband excitations by visible light. The extremely low electronic conductivity of pristine LTO means that conduction and valence bands are predominantly empty and filled, thus drastically decreasing the probability of intraband transitions. These properties of pristine LTO make it very durable against laser irradiation and explain why laser-induced degradation was not reported previously.

Doping drastically changes the optical properties of LTO. It loses its exceptionally white color, its electronic conductivity grows, and the bandgap becomes narrower [16,39]. The probability of both intraband and interband excitation by visible light significantly increases. This free-carrier absorption provides energy, which destabilizes chemical bonds directly from electronic excitation [40]. We think that some part of this absorbed energy is transferred into heat, but this effect is minor since we do not see Raman band shifts and broadening (Figure S4). The bond destabilization in a large volume of irradiated particles can result in the loss of long-range order or, in other words, laser-induced amorphization of crystalline LTO particles.

A similar effect of laser-induced amorphization is also observed in conventional semiconductors [41,42]. Amorphization is a common result of laser action during Raman measurements, but since it can be revealed mainly by the decreased Raman intensity, it is usually not reported. In most cases, Raman studies are made in powder, so the measured spectra contain the collective response of many particles [43–47]. The decrease in Raman response from one amorphizing particle is somehow concealed by the responses from underneath layers and nearby particles. We suppose that bond destabilization is more likely to happen near imperfections, such as defects and grain boundaries. The presence of copper substrate can significantly accelerate the chemical bond destabilization. The surface roughness of the copper substrate can amplify the electromagnetic field of the probing laser by localized plasmons, thus enhancing laser-induced transformation [48].

Please note that the observed degradation processes for $\text{Li}_{3.95}\text{Mn}_{0.05}\text{Ti}_5\text{O}_{12}$ differ drastically from ones, reported earlier for LiFePO_4 , another oxide, used as an electrode

material for lithium batteries. Even though authors have concluded about laser-induced amorphization for one of studied LFP particle [7], the dominating result of laser irradiation was decomposition with the formation of decomposition products. The SEM images revealed not the ablation but the partial or complete melting-down of the decomposed LFP particle, not observed for $\text{Li}_{3.95}\text{Mn}_{0.05}\text{Ti}_5\text{O}_{12}$.

4.2.2. Stimulated Transport of Molecules and Ions into the Volume of Irradiated Particles

The most intriguing processes happened after the stimulated Mn-doped LTO amorphization. The formation of amorphized regions around imperfections may enable transport of molecules from the particle surface to the bulk, and the obtained results showed that this process continued even after switching the laser irradiation off. We suppose that the remnant water layer at the copper substrate can be the main reason behind the slow degradation processes taking place between measurements. The following explanation is based on the presence of water, but the similar transport of molecules and ions can be supposed for other forms of sample contamination. The main accent was made on water since it can be found on a surface of almost any material in contact with the atmosphere [49].

Although Raman spectra measurements were performed in the atmosphere with relative humidity <10%, the copper substrate was previously exposed to an ambient atmosphere with relative humidity up to 30–50%. The substrate surface was not dried using argon plasma etching, so some remnant layer of water was natural [50–52]. When a particle was deposited at a substrate with a water layer, the capillary effect led to the formation of a meniscus (see, for example, [50,51,53]), thus increasing the area of the particle–water interface. The thickness of the water layer/meniscus was expected to be few monolayers either in ice-like (ordered) [53,54] or liquid [55] states.

In the case of solid-state synthesis, particles are polycrystals with some fraction of grain boundaries and defects. We assumed that laser irradiation increased the fraction of imperfections in the particles. These interphases and imperfections may act as channels for water transport from the surface into the particle bulk. The pattern of grain boundaries and imperfections is a fingerprint of the particle under study, and its concentration and location relative to the substrate vary from particle to particle.

The water-induced degradation of LB electrode material is rather common but supposed to be too slow to have a notable effect on the properties of the particle under study (or powder in general). However, during RS probing, such a particle being in contact with the remnant water layer is exposed to the action of laser irradiation. The penetration depth of laser beam is not well studied for LTO but keeping in mind the relatively small sizes of studied particles and results obtained for LiFePO_4 [43], let us assume that some amount of laser irradiation reached the copper substrate underneath Mn-LTO particles. This laser radiation was partially absorbed, thus heating both substrate and contiguous water layer. Regardless of its initial state (ice-like or liquid), this combined excitation by laser irradiation and heat accelerates the transport of water or its products into the particle bulk, thus initiating degradation processes not only in the point of contact but also in its vicinity.

Besides increasing the water molecules transport via grain boundaries, there are some other possible effects of the combined action of laser irradiation and water. Water could better penetrate through grain boundaries in the form of H_3O^+ and OH^- ions, resulting from the electric-field-induced dissociation of water [56,57]. In addition, laser radiation may stimulate the formation of CH_4 and other hydrocarbons due to the reduction of ambient CO_2 on a copper substrate in the presence of water [58]. In these terms, the copper substrate could stimulate not only physical laser-induced processes but also chemical ones.

4.2.3. Combined Result of Fast and Slow Stimulated Processes

We could hardly describe all the possible chemical reactions stimulated by laser irradiation and the copper substrate in and near Mn-doped LTO in the presence of water and ambient atmosphere, but we suppose that these induced transformations consist of a series of fast and slow processes.

Before the action of laser irradiation, the system Mn:LTO particle–copper substrate–water meniscus–air is in equilibrium or, at least, in the metastable state (Figure 4a). Primary laser action during Raman measurement initiates two processes (among others): a fast physical process of partial amorphization for the whole particle and slow chemical processes at the triple point particle–water–air in the vicinity of the copper substrate (Figure 4b). After switching the laser radiation off, the fast physical process ends but slow chemical processes continue (Figure 4c). Possibly, this is because the catalytic action of the copper substrate remaining active even without laser irradiation.

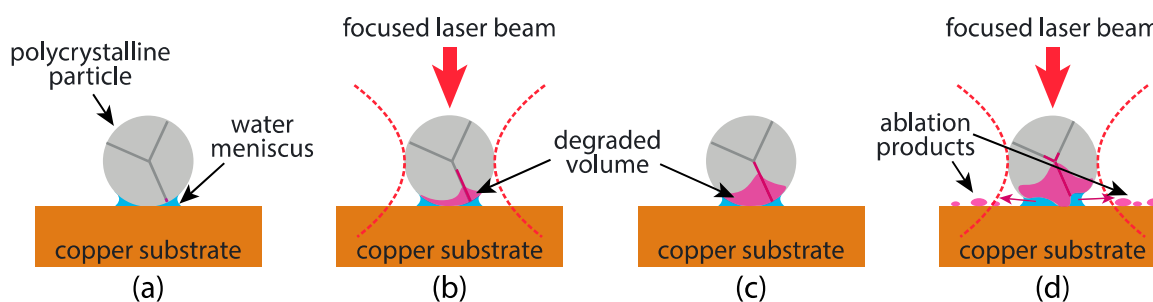


Figure 4. Schematic illustration of the laser-stimulated degradation of a polycrystalline particle on a copper substrate: (a) before the initial measurement, (b) during the first laser action, (c) after the first laser action, (d) during the repeated measurement. The dotted red line illustrates the geometry of the laser beam.

The following secondary action of laser radiation affects the altered particle, so the result of the same action may differ from the primary one. Besides further laser-induced amorphization, one should consider the action of laser irradiation on the products of a chemical reaction. The amount of decomposition product should vary from particle to particle due to the variation of water meniscus size, the concentration of the grain boundaries (or other defects) near the triple boundary point (Figure 4), and the variation of laser–matter interactions [43]. In some cases (particles #5 and #10 for the first series of measurements), this amount is enough to initiate the fast physical process of laser ablation of the decomposition products (Figure 4d), while in other cases, it was not insufficient (particles #4 and #8).

4.2.4. Laser Ablation of Decomposition Products

The laser ablation of the decomposition products but not LTO itself explains the coexistence of the particle with unchanged morphology and nanoobjects nearby (compare Figure 3d,f and Figure 4d). For example, LiFePO_4 particles also degraded under the action of laser irradiation, but its surface changed notably, and laser ablation products were not observed [7]. Since the Mn-LTO particle interacts with water meniscus at the vicinity of the particle–substrate contact point, the supposed local decomposition should take place in its bottom part, while its upper part, visualized by SEM, remains undamaged.

Ablation products were distributed nonuniformly near particle #10 (Figure 3f) and almost uniformly near particle #5 (Figure 3d) and all the particles in the verification group for the second series of measurements (Figures S15–S24). Moreover, in the case of the verification group, the nanoparticles attributed to ablation products can be found not only near LTO particles but even on them. This peculiarity can be easily explained by the redeposition of ablation products.

The nonuniform pattern was observed for particle #10, which degraded during the final action of laser irradiation with the maximal power. This nonuniform pattern may somehow correspond to the nonuniformity of grain boundaries near the substrate or multiple contact points with water meniscuses. Particle #5 degraded at 4.1 mW, and after this, it was irradiated one more time with a laser power of 4.9 mW. The particles in the verification group of the second series of measurements were subjected to numerous

irradiations with varied power. So even if the initial patterns of ablation products were unique for each particle, the repeated laser irradiation made these patterns more uniform, covering the particles themselves.

4.2.5. Possible Laser-Induced Crystallization

The action of laser irradiation on semiconductors can induce both the amorphization of crystalline materials and the crystallization of amorphous ones [59]. In our case, we did not observe the reverse crystallization of amorphized particles but could suppose a kind of laser-induced “rejuvenation.” First, we can mention particles #23 and #38 (Figures S6 and S13), which were supposed to be partially degraded but lately somehow restored their Raman spectra. In addition, particles #28, #29, and #33 worsened in some experiments but lately improved (Figures S8, S9 and S11).

We suppose that the effect of laser-induced rejuvenation of partially amorphized LTO particles is possible but not so pronounced, especially for the verification group with its exposition to large laser irradiation. We suppose that the reversibility of physical transformations is largely overbalanced by the irreversibility of the induced chemical processes.

4.2.6. The Discussion about Further Verifications of the Proposed Physicochemical Model

In this work we suppose the essential role of the surface water layer in the observed laser-induced degradation. At the same time, as we noted in the beginning of Section 4.2.2, the proposed explanation is suitable for other forms of surface contamination or gases in the atmosphere. The emphasis is made on the water layer since it is a common reason for lithium battery material degradation. Its presence is expected in most experiments, but its role is often underestimated.

The verification experiment for the dried sample in the inert atmosphere is obviously eligible but was not conducted in this work for several reasons. First, the objective of this experimental work is to report the degradation of doped LTO. The purpose of Section 4.2, proposing a physicochemical model is not the close the discussion, but to open it.

Another important point is that the study of the degradation processes without presence of the water layer is possible, but this will be another experiment studying other physicochemical processes. As it was shown earlier, the Raman study of LTO in inert atmosphere induces changes in its Raman spectra, possibly, due to a laser-induced oxygen non-stoichiometry [20]. The same problem is with a sample dehydration. To clean the surface of a substrate, one should better use argon plasma etching. It is not clear who is to completely remove a water from a powder sample and how this dehydration will change the properties of the studied sample. We are welcome water-free experiments but would like to warn that such an experiment requires very careful preparation.

4.3. Possible Implications

How can the results demonstrated in this work be used by other research groups? Let us mention three recommendations.

First, even though Raman spectroscopy cannot be considered a nondestructive characterization tool for doped LTO, it still can be used for structural studies. If the degradation of some studied volume is not crucial, researchers can use a safe laser power. The only point is that some unidentified Raman spectra can be attributed to degradation products or substrates.

Second, the main issue of slow laser-induced degradation is that it complicates the use and interpretation of in-situ Raman experiments. Although we do not know the possible laser-induced chemical reactions when the particle under study is surrounded not by air but by electrolytes, one can still suppose the presence of slow degradation processes, which may become significant for long lasting electrochemical studies. To avoid the misinterpretation of results, one should study possible degradation processes under specific conditions.

Third, we believe that besides limitations and obstacles, laser-induced degradation can be used as a convenient model to understand other forms of degradations, for example,

thermal degradation [60] or gassing during cycling [61], especially ones taking place in the vicinity of copper current collectors.

5. Conclusions

A single-particle approach with the correlative analysis of the Raman spectra and SEM images made it possible to reveal that the laser-induced degradation of Mn-doped lithium titanate is fundamentally different from that of lithium-iron phosphates, reported by us earlier. In the case of $\text{Li}_{3.95}\text{Mn}_{0.05}\text{Ti}_5\text{O}_{12}$, the observed laser-induced degradation consists of fast and slow processes. We suppose that the action of laser irradiation during Raman probing results in partial nonthermal amorphization in the vicinity of grain boundaries and other imperfections via direct bond destabilization. Besides direct laser-induced degradation, the accelerated water transport from the meniscus at the contact point of particles with the copper substrate into the particle bulk. The repeated action of the laser irradiation may result in the laser ablation of the degradation products observed as a nanoparticulate pattern around the particles.

Since the laser irradiation as an excitation only stimulates and accelerates phase transitions, but does not define its pathways, we can suppose that the preferable route of LTO alteration is the formation of amorphous phases rather than crystalline decomposition products. This is an important finding since these amorphous phases are hard to detect by conventional characterization techniques. This supposition requires further verification, and we have demonstrated this can be done by the proposed single particle approach, which allows us to study laser-induced amorphization and the following ablation of the degradation products. In addition, the reported findings may be used for the study of degradation processes during heating or prolonged electrochemical cycling.

Supplementary Materials: The following supporting information can be downloaded at: <https://www.mdpi.com/article/10.3390/batteries8120251/s1>, Figure S1: Raman spectra measured at two-month intervals for (a) “stable” particle #8, and (b) particle #10, degraded during repeated measurement, and particles (c) #13 and (d) #19, degraded between initial and repeated measurements; Figure S2. Rescaled Raman spectra measured at two-month intervals for “stable” particles (a) #4 and (b) #8, particles (c) #6 and (d) #19, degraded between initial and repeated measurements, and particles (e) #5 and (f) #10, degraded during repeated measurement; Figure S3. Raman spectra evolution with the probing laser power growth for particles #5 and #10, degraded during measurement; Figure S4. The dependence of Raman spectra parameters on the laser power for five single particles; Figures S5–S24. The evolution of Raman spectra for various particles. Figure S25. Comparison of (a,d) LTO, (b,e) LCO, and (c,f) LFP particles on a copper substrate after laser-induced degradation.

Author Contributions: Conceptualization, D.V.P.; methodology, D.V.P. and A.A.N.; software, A.A.N.; validation, R.N.N., K.G. and S.-k.L.; formal analysis, D.V.P. and S.-k.L.; investigation, A.A.N.; resources, D.V.P., R.N.N., K.G. and S.-k.L.; data curation, D.V.P.; writing—original draft preparation, D.V.P.; writing—review and editing, S.-k.L.; visualization, D.K.K. and A.A.N.; supervision, D.V.P.; project administration, D.V.P.; funding acquisition, D.V.P. and S.-k.L. All authors have read and agreed to the published version of the manuscript.

Funding: The research was funded by the Russian Science Foundation (project No 22-22-00350, <https://rscf.ru/project/22-22-00350>). The Raman spectra measurement and SEM imaging were made using equipment of the Ural Center for Shared Use “Modern nanotechnology” Ural Federal University (Reg. No 2968), supported by the Ministry of Science and Higher Education of the Russian Federation (Project No 075-15-2021-677). K.G. and S.-k.-L. gratefully acknowledge the financial supports from the Ministry of Science and Technology (MOST) in Taiwan (111-2636-E-006-018 and 110-2923-E-006-011).

Data Availability Statement: The datasets generated during and analyzed during the current study are available from the corresponding author on reasonable request.

Acknowledgments: Authors warmly thank Vadim S. Gorshkov for the highly productive discussion.

Conflicts of Interest: The authors declare no conflict of interest.

References

1. Landmarks Timeline. Available online: <https://www.acs.org/content/acs/en/education/whatischemistry/landmarks/landmarks-timeline.html> (accessed on 10 August 2020).
2. Burba, C.M.; Palmer, J.M.; Holinsworth, B.S. Laser-induced phase changes in olivine FePO₄: A warning on characterizing LiFePO₄-based cathodes with Raman spectroscopy. *J. Raman Spectrosc.* **2009**, *40*, 225–228. [[CrossRef](#)]
3. Galinetto, P.; Mozzati, M.C.; Grandi, M.S.; Bini, M.; Capsoni, D.; Ferrari, S.; Massarotti, V. Phase stability and homogeneity in undoped and Mn-doped LiFePO₄ under laser heating. *J. Raman Spectrosc.* **2010**, *41*, 1276–1282. [[CrossRef](#)]
4. Markevich, E.; Sharabi, R.; Haik, O.; Borgel, V.; Salitra, G.; Aurbach, D.; Semrau, G.; Schmidt, M.A.; Schall, N.; Stinner, C. Raman spectroscopy of carbon-coated LiCoPO₄ and LiFePO₄ olivines. *J. Power Sources* **2011**, *196*, 6433–6439. [[CrossRef](#)]
5. Bai, Y.; Yin, Y.; Yang, J.; Qing, C.; Zhang, W. Raman study of pure, C-coated and Co-doped LiFePO₄: Thermal effect and phase stability upon laser heating. *J. Raman Spectrosc.* **2011**, *42*, 831–838. [[CrossRef](#)]
6. Ryabin, A.A.; Slautin, B.N.; Pelegov, D.V. Three-stage kinetics of laser-induced LiFePO₄ decomposition. *J. Raman Spectrosc.* **2020**, *51*, 528–536. [[CrossRef](#)]
7. Ryabin, A.A.; Pelegov, D.V. An ambiguity of laser-induced degradation in LiFePO₄ and advantages of single-particle approach to Raman spectroscopy. *J. Raman Spectrosc.* **2022**, *53*, 1625–1634. [[CrossRef](#)]
8. Song, S.W.; Han, K.S.; Fujita, H.; Yoshimura, M. In situ visible Raman spectroscopic study of phase change in LiCoO₂ film by laser irradiation. *Chem. Phys. Lett.* **2001**, *344*, 299–304. [[CrossRef](#)]
9. Kohler, R.; Proell, J.; Ulrich, S.; Trouillet, V.; Indris, S.; Przybylski, M.; Pflöging, W. Laser-assisted structuring and modification of LiCoO₂ thin films. *SPIE—Int. Soc. Opt. Eng.* **2009**, *7202*, 69–79.
10. Ruther, R.E.; Callender, A.F.; Zhou, H.; Martha, S.K.; Nanda, J. Raman Microscopy of Lithium-Manganese-Rich Transition Metal Oxide Cathodes. *J. Electrochem. Soc.* **2015**, *162*, A98–A102. [[CrossRef](#)]
11. Paolone, A.; Sacchetti, A.; Corridoni, T.; Postorino, P.; Cantelli, R.; Rousse, G.; Masquelier, C. MicroRaman spectroscopy on LiMn₂O₄: Warnings on laser-induced thermal decomposition. *Solid State Ion.* **2004**, *170*, 135–138. [[CrossRef](#)]
12. Bernardini, S.; Bellatreccia, F.; Della Ventura, G.; Ballirano, P.; Sodo, A. Raman spectroscopy and laser-induced degradation of groutellite and ramsdellite, two cathode materials of technological interest. *RSC Adv.* **2020**, *10*, 923–929. [[CrossRef](#)] [[PubMed](#)]
13. Capsoni, D.; Bini, M.; Massarotti, V.; Mustarelli, P.; Chiodelli, G.; Azzoni, C.B.; Mozzati, M.C.; Linati, L.; Ferrari, S. Cations Distribution and Valence States in Mn-Substituted Li₄Ti₅O₁₂ Structure. *Chem. Mater.* **2008**, *20*, 4291–4298. [[CrossRef](#)]
14. Nithya, V.D.; Kalai Selvan, R.; VEDIAPPAN, K.; Sharmila, S.; Lee, C.W. Molten salt synthesis and characterization of Li₄Ti₅–xMnxO₁₂ (x = 0.0, 0.05 and 0.1) as anodes for Li-ion batteries. *Appl. Surf. Sci.* **2012**, *261*, 515–519. [[CrossRef](#)]
15. Kaftelen, H.; Tuncer, M.; Tu, S.; Repp, S.; Göçmez, H.; Thomann, R.; Weber, S.; Erdem, E. Mn-substituted spinel Li₄Ti₅O₁₂ materials studied by multifrequency EPR spectroscopy. *J. Mater. Chem. A* **2013**, *1*, 9973. [[CrossRef](#)]
16. Singh, H.; Topsakal, M.; Attenkofer, K.; Wolf, T.; Leskes, M.; Duan, Y.; Wang, F.; Vinson, J.; Lu, D.; Frenkel, A.I. Identification of dopant site and its effect on electrochemical activity in Mn-doped lithium titanate. *Phys. Rev. Mater.* **2018**, *2*, 125403. [[CrossRef](#)] [[PubMed](#)]
17. Leonidov, I.A.; Leonidova, O.N.; Perelyaeva, L.A.; Samigullina, R.F.; Kovyazina, S.A.; Patrakeev, M.V. Structure, ionic conduction, and phase transformations in lithium titanate Li₄Ti₅O₁₂. *Phys. Solid State* **2003**, *45*, 2183–2188. [[CrossRef](#)]
18. Julien, C.M.; Massot, M.; Zaghib, K. Structural studies of Li_{4/3}Me_{5/3}O₄ (Me = Ti, Mn) electrode materials: Local structure and electrochemical aspects. *J. Power Sources* **2004**, *136*, 72–79. [[CrossRef](#)]
19. Aldon, L.; Kubiak, P.; Womes, M.; Jumas, J.C.; Olivier-Fourcade, J.; Tirado, J.L.; Corredor, J.I.; Pérez Vicente, C. Chemical and Electrochemical Li-Insertion into the Li₄Ti₅O₁₂ Spinel. *Chem. Mater.* **2004**, *16*, 5721–5725. [[CrossRef](#)]
20. Pelegov, D.V.; Slautin, B.N.; Gorshkov, V.S.; Zelenovskiy, P.S.; Kiselev, E.A.; Kholkin, A.L.; Shur, V.Y. Raman spectroscopy, “big data”, and local heterogeneity of solid state synthesized lithium titanate. *J. Power Sources* **2017**, *346*, 143–150. [[CrossRef](#)]
21. Pelegov, D.V.; Nasara, R.N.; Tu, C.; Lin, S. Defects in Li₄Ti₅O₁₂ induced by carbon deposition: An analysis of unidentified bands in Raman spectra. *Phys. Chem. Chem. Phys.* **2019**, *21*, 20757–20763. [[CrossRef](#)] [[PubMed](#)]
22. Mukai, K.; Kato, Y. Role of Oxide Ions in Thermally Activated Lithium Diffusion of Li[Li_{1/3}Ti_{5/3}]O₄: X-ray Diffraction Measurements and Raman Spectroscopy. *J. Phys. Chem. C* **2015**, *119*, 10273–10281. [[CrossRef](#)]
23. Chan, H.Y.H.; Takoudis, C.G.; Weaver, M.J. Oxide Film Formation and Oxygen Adsorption on Copper in Aqueous Media As Probed by Surface-Enhanced Raman Spectroscopy. *J. Phys. Chem. B* **1999**, *103*, 357–365. [[CrossRef](#)]
24. Deng, Y.; Handoko, A.D.; Du, Y.; Xi, S.; Yeo, B.S. In Situ Raman Spectroscopy of Copper and Copper Oxide Surfaces during Electrochemical Oxygen Evolution Reaction: Identification of Cu III Oxides as Catalytically Active Species. *ACS Catal.* **2016**, *6*, 2473–2481. [[CrossRef](#)]
25. Michalska, M.; Krajewski, M.; Ziolkowska, D.; Hamankiewicz, B.; Andrzejczuk, M.; Lipinska, L.; Korona, K.P.; Czerwinski, A. Influence of milling time in solid-state synthesis on structure, morphology and electrochemical properties of Li₄Ti₅O₁₂ of spinel structure. *Powder Technol.* **2014**, *266*, 372–377. [[CrossRef](#)]
26. Knyazev, A.V.; Smirnova, N.N.; Mączka, M.; Knyazeva, S.S.; Letyanina, I.A. Thermodynamic and spectroscopic properties of spinel with the formula Li_{4/3}Ti_{5/3}O₄. *Thermochim. Acta* **2013**, *559*, 40–45. [[CrossRef](#)]
27. Yue, J.; Suchomski, C.; Brezesinski, T.; Smarsly, B.M. Polymer-Templated Mesoporous Li₄Ti₅O₁₂ as a High-Rate and Long-Life Anode Material for Rechargeable Li-Ion Batteries. *ChemNanoMat* **2015**, *1*, 415–421. [[CrossRef](#)]
28. Zhao, Q.; Zhou, J.; Zhang, F.; Lippens, D. Mie resonance-based dielectric metamaterials. *Mater. Today* **2009**, *12*, 60–69. [[CrossRef](#)]

29. Pendry, J.B. Controlling Electromagnetic Fields. *Science* **2006**, *312*, 1780–1782. [[CrossRef](#)]
30. Tzarouchis, D.; Sihvola, A. Light Scattering by a Dielectric Sphere: Perspectives on the Mie Resonances. *Appl. Sci.* **2018**, *8*, 184. [[CrossRef](#)]
31. Xia, X.; Wang, Z.; Chen, L. Regeneration and characterization of air-oxidized LiFePO₄. *Electrochem. Commun.* **2008**, *10*, 1442–1444. [[CrossRef](#)]
32. Ziolkowska, D.; Korona, K.P.; Hamankiewicz, B.; Wu, S.-H.; Chen, M.-S.; Jasinski, J.B.; Kaminska, M.; Czerwinski, A. The role of SnO₂ surface coating on the electrochemical performance of LiFePO₄ cathode materials. *Electrochim. Acta* **2013**, *108*, 532–539. [[CrossRef](#)]
33. Jugović, D.; Mitrić, M.; Milović, M.; Cvjetičanin, N.; Jokić, B.; Umičević, A.; Uskoković, D. The influence of fluorine doping on the structural and electrical properties of the LiFePO₄ powder. *Ceram. Int.* **2017**, *43*, 3224–3230. [[CrossRef](#)]
34. Lazarević, Z.Ž.; Križan, G.; Križan, J.; Milutinović, A.; Ivanovski, V.N.; Mitrić, M.; Gilić, M.; Umičević, A.; Kuryliszyn-Kudelska, I.; Romčević, N.Ž. Characterization of LiFePO₄ samples obtained by pulse combustion under various conditions of synthesis. *J. Appl. Phys.* **2019**, *126*, 085109. [[CrossRef](#)]
35. Mukai, K.; Kato, Y.; Nakano, H. Understanding the Zero-Strain Lithium Insertion Scheme of Li[Li_{1/3}Ti_{5/3}]O₄: Structural Changes at Atomic Scale Clarified by Raman Spectroscopy. *J. Phys. Chem. C* **2014**, *118*, 2992–2999. [[CrossRef](#)]
36. Pelegov, D.V.; Slautin, B.N.; Zelenovskiy, P.S.; Kuznetsov, D.K.; Kiselev, E.A.; Alikin, D.O.; Kholkin, A.L.; Shur, V.Y. Single particle structure characterization of solid-state synthesized Li₄Ti₅O₁₂. *J. Raman Spectrosc.* **2017**, *48*, 278–283. [[CrossRef](#)]
37. Ohsaka, T.; Izumi, F.; Fujiki, Y. Raman spectrum of anatase, TiO₂. *J. Raman Spectrosc.* **1978**, *7*, 321–324. [[CrossRef](#)]
38. Swamy, V.; Kuznetsov, A.; Dubrovinsky, L.S.; Caruso, R.A.; Shchukin, D.G.; Muddle, B.C. Finite-size and pressure effects on the Raman spectrum of nanocrystalline anatase TiO₂. *Phys. Rev. B-Condens. Matter Mater. Phys.* **2005**, *71*, 184302. [[CrossRef](#)]
39. Nasara, R.N.; Lin, S. Recent Developments in Using Computational Materials Design for High-Performance Li₄Ti₅O₁₂ Anode Material for Lithium-Ion Batteries. *Multiscale Sci. Eng.* **2019**, *1*, 87–107. [[CrossRef](#)]
40. Siegal, Y.; Glezer, E.N.; Huang, L.; Mazur, E. Laser-Induced Phase Transitions in Semiconductors. *Annu. Rev. Mater. Sci.* **1995**, *25*, 223–247. [[CrossRef](#)]
41. Yen, R.; Liu, J.M.; Kurz, H.; Bloembergen, N. Space-time resolved reflectivity measurements of picosecond laser-pulse induced phase transitions in (111) silicon surface layers. *Appl. Phys. A Solids Surfaces* **1982**, *27*, 153–160. [[CrossRef](#)]
42. Bonse, J.; Brzezinka, K.-W.; Meixner, A. Modifying single-crystalline silicon by femtosecond laser pulses: An analysis by micro Raman spectroscopy, scanning laser microscopy and atomic force microscopy. *Appl. Surf. Sci.* **2004**, *221*, 215–230. [[CrossRef](#)]
43. Ryabin, A.A.; Pelegov, D.V. Spatial Resolution of Micro-Raman Spectroscopy for Particulate Lithium Iron Phosphate (LiFePO₄). *Appl. Spectrosc.* **2022**, *76*, 1335–1345. [[CrossRef](#)] [[PubMed](#)]
44. Foucher, F.; Guimbretière, G.; Bost, N.; Westall, F. Petrographical and Mineralogical Applications of Raman Mapping. In *Raman Spectroscopy and Applications*; InTech: London, UK, 2017.
45. Foucher, F. Influence of laser shape on thermal increase during micro-Raman spectroscopy analyses. *J. Raman Spectrosc.* **2022**, *53*, 664–676. [[CrossRef](#)]
46. Overall, N.J. Confocal Raman microscopy: Common errors and artefacts. *Analyst* **2010**, *135*, 2512–2522. [[CrossRef](#)] [[PubMed](#)]
47. Overall, N.J. Confocal Raman Microscopy: Why the Depth Resolution and Spatial Accuracy Can Be Much Worse Than You Think. *Appl. Spectrosc.* **2000**, *54*, 1515–1520. [[CrossRef](#)]
48. Csarnovics, I.; Veres, M.; Nemeč, P.; Molnár, S.; Kókényesi, S. Surface plasmon enhanced light-induced changes in Ge-Se amorphous chalcogenide-gold nanostructures. *J. Non-Cryst. Solids* **2021**, *553*, 120491. [[CrossRef](#)]
49. Summer, A.L.; Menke, E.J.; Dubowski, Y.; Newberg, J.T.; Penner, R.M.; Hemminger, J.C.; Wingen, L.M.; Brauers, T.; Finlayson-Pitts, B.J. The nature of water on surfaces of laboratory systems and implications for heterogeneous chemistry in the troposphere. *Phys. Chem. Chem. Phys.* **2004**, *6*, 604. [[CrossRef](#)]
50. Rabinovich, Y.I.; Adler, J.J.; Esayanur, M.S.; Ata, A.; Singh, R.K.; Moudgil, B.M. Capillary forces between surfaces with nanoscale roughness. *Adv. Colloid Interface Sci.* **2002**, *96*, 213–230. [[CrossRef](#)]
51. Butt, H.-J.; Kappl, M. Normal capillary forces. *Adv. Colloid Interface Sci.* **2009**, *146*, 48–60. [[CrossRef](#)] [[PubMed](#)]
52. Maier, S.; Salmeron, M. How Does Water Wet a Surface? *Acc. Chem. Res.* **2015**, *48*, 2783–2790. [[CrossRef](#)] [[PubMed](#)]
53. Weeks, B.L.; Vaughn, M.W.; DeYoreo, J.J. Direct Imaging of Meniscus Formation in Atomic Force Microscopy Using Environmental Scanning Electron Microscopy. *Langmuir* **2005**, *21*, 8096–8098. [[CrossRef](#)]
54. Asay, D.B.; Kim, S.H. Effects of adsorbed water layer structure on adhesion force of silicon oxide nanoasperity contact in humid ambient. *J. Chem. Phys.* **2006**, *124*, 174712. [[CrossRef](#)] [[PubMed](#)]
55. Barthel, A.J.; Kim, S.H. Surface chemistry dependence of water adsorption on solid substrates in humid ambient and humidity effects on wear of copper and glass surfaces. *Tribol.-Mater. Surfaces Interfaces* **2013**, *7*, 63–68. [[CrossRef](#)]
56. Geissler, P.L.; Dellago, C.; Chandler, D.; Hutter, J.; Parrinello, M. Autoionization in Liquid Water. *Science* **2001**, *291*, 2121–2124. [[CrossRef](#)] [[PubMed](#)]
57. Zhou, K.-G.; Vasu, K.S.; Cherian, C.T.; Neek-Amal, M.; Zhang, J.C.; Ghorbanfekr-Kalashami, H.; Huang, K.; Marshall, O.P.; Kravets, V.G.; Abraham, J.; et al. Electrically controlled water permeation through graphene oxide membranes. *Nature* **2018**, *559*, 236–240. [[CrossRef](#)] [[PubMed](#)]
58. Belharouak, I.; Koenig, G.M.; Tan, T.; Yumoto, H.; Ota, N.; Amine, K. Performance Degradation and Gassing of Li₄Ti₅O₁₂/LiMn₂O₄ Lithium-Ion Cells. *J. Electrochem. Soc.* **2012**, *159*, A1165–A1170. [[CrossRef](#)]

59. Akhmanov, S.A.; Emel'yanov, V.I.; Koroteev, N.I.; Seminogov, V.N. Interaction of powerful laser radiation with the surfaces of semiconductors and metals: Nonlinear optical effects and nonlinear optical diagnostics. *Sov. Phys. Uspekhi* **1985**, *28*, 1084–1124. [[CrossRef](#)]
60. Wu, K.; Yang, J.; Zhang, Y.; Wang, C.; Wang, D. Investigation on $\text{Li}_4\text{Ti}_5\text{O}_{12}$ batteries developed for hybrid electric vehicle. *J. Appl. Electrochem.* **2012**, *42*, 989–995. [[CrossRef](#)]
61. Han, C.; He, Y.-B.; Liu, M.; Li, B.; Yang, Q.-H.; Wong, C.-P.; Kang, F. A review of gassing behavior in $\text{Li}_4\text{Ti}_5\text{O}_{12}$ -based lithium ion batteries. *J. Mater. Chem. A* **2017**, *5*, 6368–6381. [[CrossRef](#)]